JACS
JOURNAL OF THE AMERICAN CHEMICAL SOCIETY
Article
pubs.acs.org/JACS

Highly Tunable Molecular Sieving and Adsorption Properties of Mixed-Linker Zeolitic Imidazolate Frameworks

Kiwon Eum,[†,∥] Krishna C. Jayachandrababu,[†,∥] Fereshteh Rashidi,[†,∥] Ke Zhang,[†,∥] Johannes Leisen,[‡] Samuel Graham,[§] Ryan P. Lively,[†] Ronald R. Chance,[†] David S. Sholl,[†] Christopher W. Jones,[†,‡] and Sankar Nair*[,†]

[†]School of Chemical & Biomolecular Engineering, Georgia Institute of Technology, Atlanta, Georgia 30332-0100, United States
[‡]School of Chemistry and Biochemistry, Georgia Institute of Technology, Atlanta, Georgia 30332-0400, United States
[§]Woodruff School of Mechanical Engineering, Georgia Institute of Technology, Atlanta, Georgia 30332-0405, United States

Supporting Information

ABSTRACT: Nanoporous zeolitic imidazolate frameworks (ZIFs) form structural topologies equivalent to zeolites. ZIFs containing only one type of imidazole linker show separation capability for limited molecular pairs. We show that the effective pore size, hydrophilicity, and organophilicity of ZIFs can be continuously and drastically tuned using mixed-linker ZIFs containing two types of linkers, allowing their use as a more general molecular separation platform. We illustrate this remarkable behavior by adsorption and diffusion measurements of hydrocarbons, alcohols, and water in mixed-linker ZIF-8_x-90_{100-x} materials with a large range of crystal sizes (338 nm to 120 μm), using volumetric, gravimetric, and PFG-NMR methods. NMR, powder FT-Raman, and micro-Raman spectroscopy unambiguously confirm the mixed-linker nature of individual ZIF crystals. Variation of the mixed-linker composition parameter (x) allows continuous control of *n*-butane, *i*-butane, butanol, and isobutanol diffusivities over 2−3 orders of magnitude and control of water and alcohol adsorption especially at low activities.

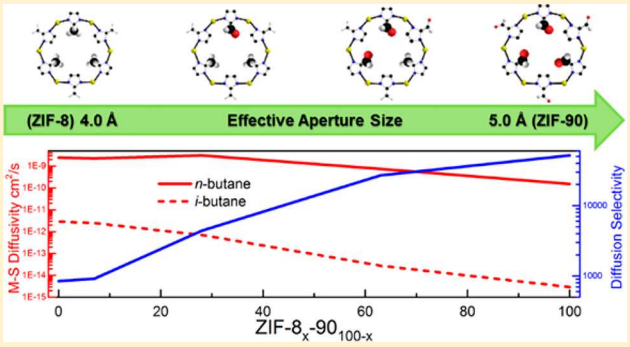

INTRODUCTION

Metal organic frameworks (MOFs) are nanoporous materials consisting of organic linkers coordinated to metal ions in crystalline structures. They are potentially attractive as energy-efficient gas separation materials and membranes.[1] MOFs can be used for separations by exploiting differences in molecular adsorption strength, diffusivity, or both.[2] The vast range of MOF structures and the relative simplicity of their synthesis (compared to other nanoporous materials like zeolites) create the possibility of rational design, synthesis, and modification of MOF structures[3,4] for specific adsorptive[5−7] or diffusion-based[8−11] separations. A subclass of MOFs, known as zeolitic imidazolate frameworks (ZIFs), consists of metal (mainly tetrahedral Zn^{2+}) bridged by the nitrogen atoms of imidazolate linkers. ZIFs form structural topologies equivalent to those found in zeolites and other inorganic nanoporous oxide materials. More than 100 ZIF structures have been synthesized, including crystal topologies not realized in zeolites.[12−16] Several ZIFs are known to have good thermal and chemical stability, high microporosity, and high internal surface area.[17] ZIFs have created substantial interest for potential use in diffusive and adsorptive separations. For example, ZIF-8 is useful for membrane-based separation of hydrogen from hydrocarbons and propylene from propane to potentially replace or debottleneck energy-intensive cryogenic distillation processes.[18−20]

A considerable body of work has appeared on the quantification of molecular diffusion properties of ZIFs (most notably ZIF-8) and their use in membranes for diffusion-dominated separations.[1,21−23] It has been shown that molecules with significantly higher kinetic diameters than the nominal pore limiting diameter of ZIF-8 (3.4 Å) can diffuse through its micropores.[23] Molecular modeling and experimental measurements have shown that ZIF-8 has high diffusion selectivity for methanol over ethanol, whereas ZIF-90 has moderate selectivity for the same molecules.[24] Recent work has demonstrated the high hydrophobicity of ZIF-8 via adsorption studies of water and a number of liquid organic adsorbates.[22] ZIF-8 has also been identified as a candidate for adsorptive recovery of ethanol, propanol and butanol from water due to its hydrophobicity.[25,26]

However, it is now clear that single-linker ZIF materials can only allow "discrete" changes in pore size and adsorption characteristics by variation of the imidazolate linker. Diffusion-based molecular separations are extremely sensitive to small (<0.1 Å) changes in the effective pore size. Only limited diffusive

Received: January 26, 2015
Published: March 16, 2015

DOI: 10.1021/jacs.5b00803
J. Am. Chem. Soc. 2015, 137, 4191−4197

separations are possible with single-linker ZIFs, and *de novo* design and synthesis of ZIFs for each new separation target is difficult. Similarly, adsorptive separations are sensitive to small changes in the hydrophilicity or organophilicity of the ZIF which are difficult to design *de novo*. In previous work, we demonstrated a synthetic approach for a series of mixed-linker ZIF-8−90 and ZIF-7−8 materials by inclusion of 2-carboxyimidazole (ZIF-90 linker) and benzimidazole (ZIF-7 linker) along with 2-methylimidazole (ZIF-8 linker) during synthesis.[17,27] Preliminary characterization revealed these materials had a continuously tunable effective pore size (as measured by nitrogen physisorption) that is between the pore sizes of the single-linker "parent" materials (ZIF-7, ZIF-8, and ZIF-90). We denote the mixed-linker ZIF-8−90 materials as ZIF-8_x-90_{100-x} ($0 \leq x \leq 100$), where x is the percentage of ZIF-8 linkers in the framework. Here we demonstrate extensively that ZIF-8−90 materials have the remarkable property of continuously tunable diffusion and adsorption properties of hydrocarbons, alcohols, and water over several orders of magnitude. This result is facilitated by the controlled synthesis and characterization of a set of ZIF 8−90 mixed linker crystals spanning the entire range of 2-MeIM/OHC-IM linker ratios, and with a large and controllable range of crystal sizes (from <0.5 μm to about 100 μm). We use micro-Raman spectroscopy, as well as water adsorption isotherms, to conclusively prove the mixed-linker composition of the individual crystals. Comprehensive diffusion and adsorption measurements using PFG-NMR, gravimetric, and volumetric techniques allow a detailed demonstration and evaluation of the tunable separation properties of mixed-linker ZIFs.

EXPERIMENTAL SECTION

Materials. 2-Methylimidazole (99%, 2-MeIM), $Zn(NO_3)_2{\cdot}6H_2O$ (99%) and sodium formate (99%, $NaCO_2H$) were obtained from Sigma-Aldrich. Carboxyaldehyde-2-imidazole (99%, OHC-IM), dimethylformamide (DMF), and methanol (MeOH) were obtained from Alfa Aesar. Deionized water (DI-H_2O) was produced with a Thermo Scientific 7128 deionizer.

ZIF Synthesis. Different synthesis procedures were used to produce ZIF crystals of different size ranges suitable for hydrocarbon diffusion measurements. Each of these synthesis procedures is described in detail in the Supporting Information.

Characterization. XRD patterns were measured on a PANalytical X'Pert Pro diffractometer at room temperature using Cu Kα radiation of λ = 0.154 nm and 5−40° 2θ. Crystal size distribution (CSD) analyses were conducted with a Protein Solutions DynaPro DLS instrument, a Hitachi SU 8010 SEM, and a Nikon Eclipse 50i optical microscope. The CSD of 338 nm ZIF-8 was obtained by DLS. The ZIF-8 powder was dispersed by sonication in a filtered MeOH solution for 5 min. The colloidal suspension was inserted into a cuvette via a 5 μm syringe filter for DLS measurements. CSDs of 1−10 μm ZIF-8−90 materials were measured from multiple SEM images to obtain sample sizes of more than 200 crystals in each case. CSD of ZIF crystals >30 μm in size were obtained by optical microscopy. The samples were dispersed on a glass slide, and the CSD was measured from about 200 crystals in each case. Since large ZIF crystals are highly faceted, the equivalent spherical crystal radius was taken to be that of the smallest circle that encompasses the entire crystal. Solution ^{1}H NMR measurements were performed with a Bruker 400 MHz spectrometer after digesting the ZIF crystals in d_4-acetic acid (CD_3CO_2D). To determine the fraction of each imidazole linker in the ZIF materials, the integrated peak area of the methyl protons of 2-MeIM (chemical shift 2.65 pm) was normalized to that of the aldehyde proton of OHC-Im (9.84 pm). The chemical shifts of both imidazole linkers were referenced to the chemical shift (2.30 pm) of d_4-acetic acid. Powder FT-Raman spectroscopy was performed with a Bruker Vertex 80v FTIR/RAM II FT-Raman Analyzer in open atmosphere and a He/Ne red laser (1054 nm). Raman microscopy of individual ZIF crystals was carried out using a Horiba Jobin-Yvon HR-800 dispersive spectrometer with an 1800 l/mm grating and a green laser (532 nm). A spot size of 2.5 μm was used. Numerical integration of FT-Raman and micro-Raman peak areas was carried out with the instrument software. The 2-MeIM and OHC-IM peaks were background-subtracted using a polynomial and then fitted with mixed Gaussian−Lorentzian functions to obtain the integrated peak areas.

Adsorption and Diffusion Measurements. For pulsed field gradient (PFG) NMR measurements, samples were prepared in standard 5 mm o.d. NMR tubes. Sample loadings were calculated from adsorption isotherms given by Zhang et al.[25] Loadings were limited at 10−15% below saturation loading for all adsorbates. This range was chosen to avoid bulk condensation of liquid adsorbates in the NMR tube. The sample tubes were capped, thoroughly sealed using Parafilm, and allowed to equilibrate for 48 h before experiments were performed. The diffusivity experiments were performed using a Bruker Avance III NMR spectrometer equipped with a Diff-50 diffusion accessory operating at an ^{1}H frequency of 400 MHz. The stimulated spin echo pulse sequence was used to collect the NMR data and processed using Bruker's TopSpin software package. It was verified that the experimental conditions were chosen appropriately for measurements of intracrystalline diffusion (i.e., the average displacement of molecules during the diffusion time δ is significantly smaller than the crystal size). Adsorption isotherms for water and alcohols were collected using a VTI SA Vapor Sorption Analyzer (TA Instruments). Approximately 10−20 mg samples were used for each experiment. The samples were degassed *in situ* at 105 °C for up to 8 h in an ultrapure N_2 stream. The relative vapor pressure of each adsorbate was varied between the limits of 0.04 and 0.9 in discrete steps. Equilibrium was assumed to be achieved if less than 0.003% weight change was observed in a 5 min interval. The *n*-butane and *i*-butane transport diffusivities and adsorption isotherms were measured with a volumetric (pressure decay) apparatus.[28] A known amount of ZIF sample was sealed into a 0.5 μm filter element and installed in the sample chamber. The volumes of the sample and reservoir chambers are precisely known. It was determined that all our experiments satisfied the criterion for isothermal macroscopic diffusion.[29] The apparatus was placed in a silicone oil bath equipped with a circulator for temperature control. The sample was degassed under vacuum at 150 °C for 12 h and then maintained for 12 h at 35 °C. The vacuum was then isolated, and a known quantity of hydrocarbon gas was injected into the reservoir chamber. The valve connecting the sample and reservoir chambers was then opened. Sensitive pressure transducers attached to the sample and reservoir chambers were used to measure the pressure changes over time, occurring due to adsorption. The data were converted to uptake curves using a virial equation of state.

RESULTS AND DISCUSSION

Crystal Size Distributions. To successfully measure intracrystalline diffusivities that vary over several orders of magnitude, control over the mixed-linker ZIF-8−90 crystal size is critical. For example, the uptake of *i*-butane is slow enough to allow reliable diffusivity measurements at 35 °C with 1−10 μm crystals, whereas crystals larger than 50 μm are required to accurately measure *n*-butane diffusivities. We synthesized ZIF-8−90 mixed linker crystals of diameters ranging from 338 nm to 120 μm for uptake measurements. The mixed-linker crystals were synthesized solvothermally, and equimolar amounts of sodium formate and organic linkers were used to promote incorporation of both linkers in the framework. Thermodynamically, the Zn^{2+} metal center favors crystallization with 2-MeIM more than with OHC-IM.[30] However, in the presence of sufficient concentrations of sodium formate, both linkers will be largely deprotonated before addition of Zn^{2+} ions.[31] This allows kinetic control of the metal-linker coordination reaction and allows the formation of mixed-linker frameworks of continuously variable compositions. Figure S1 (Supporting Information) shows example SEM images of the large range of crystal sizes synthesized, and Figure S2 shows the

DOI: 10.1021/jacs.5b00803
J. Am. Chem. Soc. 2015, 137, 4191−4197

crystal size distributions obtained from DLS, SEM, or optical microscopy. The ZIF-8/ZIF-90 structure topology of all the materials was confirmed by powder XRD (Figure S3).

Crystal Composition. In general, one expects thermodynamic and kinetic differences in the incorporation of the two different linkers in the ZIF crystal structure. As a result, the percentage (x) of ZIF-8 linkers in the crystallized material is not identical to that originally present in the synthesis solution. It is therefore necessary to establish the "composition curve" that relates the two quantities and allows selection of the appropriate synthesis solution for a particular hybrid ZIF-8−90 material. Solution-phase ^{1}H NMR spectroscopy is a reliable tool for this purpose, and the composition curves thus determined are shown in Figure 1. Due to the different synthesis conditions (and hence different crystallization characteristics) used in the synthesis of "smaller" (<10 μm) and "larger" (>50 μm) ZIF-8−90 crystals, the composition curves are different for the two cases. Overall, it is seen that 2-MeIM is incorporated into the frameworks at lower fractions than present in the initial reactant solution. The data in Figure 1 are in good agreement with our initial data for small crystals of ZIF-8−90 materials.[17] Based upon the foregoing results, it is clear that ZIF-8−90 hybrids of any composition and a large range of average crystal sizes can be synthesized by the combination of techniques used in this work.

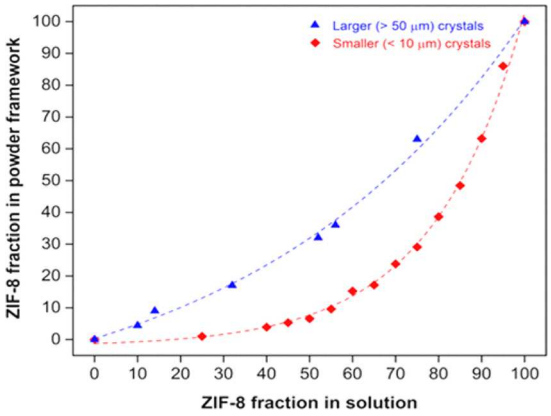

Figure 1. Composition analysis curves of ZIF-8$_x$-90$_{100-x}$ hybrid frameworks obtained by solution ^{1}H NMR. Composition curves for smaller (<10 mm) and larger (>50 mm) crystals are shown. The composition of the hybrid materials can be continuously tuned by adjusting the composition of the synthesis solution. The dashed lines are only a guide to the eye.

The XRD patterns of ZIF-8−90 materials are all essentially identical (Figure S3) because all the materials have the same framework topology and only small differences in electron density and lattice constant. In these circumstances, the slight changes in peak positions or intensities make it difficult to obtain any reliable evidence of compositional variations by XRD techniques. Previously,[17] we provided indirect evidence (via N_2 physisorption measurements) that the crystallized ZIF-8−90 materials were true hybrids and not physical mixtures of ZIF-8 and ZIF-90 crystals. However, conclusive evidence of hybrid crystal formation, as well as the distribution of the ZIF-8 linker fraction (x) across individual crystals, can only be obtained from a microanalytical technique. Here we use a comparative approach based upon micro-Raman and powder FT-Raman spectroscopy. Figure 2a shows powder FT-Raman spectra from several ZIF-8−90 materials. We use the peaks at 680 cm^{-1} (ring puckering of 2-MeIM) and 1680 cm^{-1} (C═O stretching vibration of OHC-Im) as signatures[11−13] of the ZIF-8 and ZIF-90 linkers, respectively. In addition, detailed peak assignments in the range of 1500−1100 cm^{-1} for ZIF-8 and ZIF-90, and the hybrid materials are shown in Figure S4. The ZIF-8 spectrum in this range is

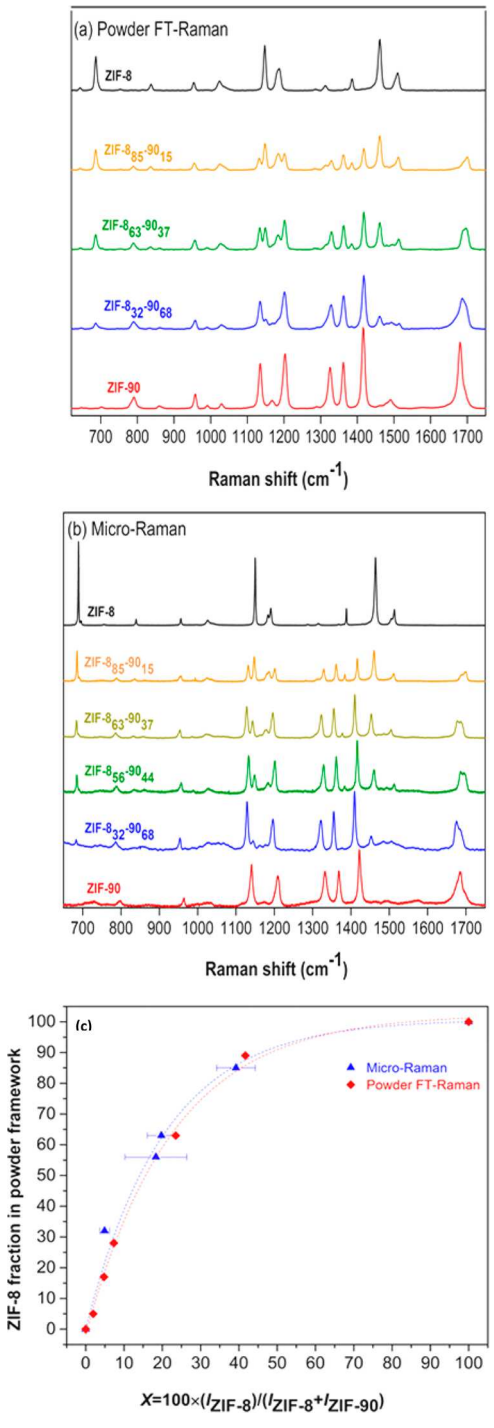

Figure 2. (a) Powder FT-Raman spectra of ZIF-8−90 hybrid framework materials, (b) micro-Raman spectra from individual ZIF-8−90 crystals, and (c) composition analysis of ZIF-8−90 hybrid crystals from FT-Raman and micro-Raman data. The quantity $X = 100 \times I_{ZIF8}/(I_{ZIF8} + I_{ZIF90})$ is obtained from the Raman measurements, whereas the quantity on the y-axis is the corresponding ZIF-8 linker fraction obtained from ^{1}H NMR. The error bars shown for the micro-Raman curve represent the standard deviation in X across at least six different crystals of the sample and three different locations in each crystal.

DOI: 10.1021/jacs.5b00803
J. Am. Chem. Soc. 2015, 137, 4191−4197

dominated by two intense peaks at 1146 and 1180 cm^{-1} corresponding to the υ_{C5-N} vibrations of the 2-MeIM ring, while the same vibrations in the ZIF-90 spectrum (OHC-IM linker) appear at 1036 and 1200 cm^{-1}. In the hybrid ZIF-8−90 frameworks, all four υ_{C5-N} peaks are observed due to the presence of both linkers. As the 2-MeIM content increases, the intensity of the OHC-IM peaks decreases, and they are eliminated in pure ZIF-8. The other peaks originating from 2-MeIM and OHC-IM also display similar behavior as a function of framework composition, namely the 2-MeIM peaks at 1370 cm^{-1} (δ_{CH_3}), 1458 cm^{-1} (δ_{C-H}), and 1499 cm^{-1} (υ_{C2-N1}) and the OHC-IM peaks at 1330 cm^{-1} (δ_{H-CO}), 1360 cm^{-1} (δ_{C-H}), and 1418 cm^{-1} (υ_{C2-N1}). These changes are consistent in both the FT-Raman and micro-Raman spectra.

We then obtain the integrated areas (I_{ZIF8} and I_{ZIF90}) of the signature peaks at 680 cm^{-1} (2-MeIM) and 1680 cm^{-1} (OHC-Im) in each FT-Raman spectrum, and use the normalized quantity $X = 100 \times I_{ZIF8}/(I_{ZIF8}+I_{ZIF90})$ as a measure of the percentage of ZIF-8 linkers in the framework. A similar procedure is carried out using micro-Raman spectra collected from at least six randomly selected individual crystals in each sample and at three different locations on each selected crystal. Figure 2b shows example micro-Raman spectra from one crystal in each ZIF-8−90 sample. The quantity X allows the cancellation of sample size effects but is not the exact equivalent of the ZIF-8 linker fraction (x) because of the different polarizabilities of the two characteristic linker vibrations. However, if the crystals are true hybrids, the "bulk" macroscopic value of X obtained from a powder FT-Raman measurement must match that obtained microscopically by micro-Raman measurements from individual crystals and locations in the sample. Moreover, a small standard deviation of X (as obtained from averaging the micro-Raman measurements over multiple crystals) would denote a highly uniform value of the ZIF-8 linker percentage x across crystals in a given powder sample. Figure 2c plots the values of X obtained from FT-Raman and micro-Raman measurements versus the values of x obtained previously from ^{1}H NMR measurements. The FT-Raman and micro-Raman techniques are in close agreement, providing clear evidence that the crystals are true mixed-linker hybrids. The generally small standard deviations (represented as horizontal error bars in Figure 2c) of X also indicate good compositional uniformity of the ZIF-8−90 crystals. It is important to note that the above discussion does not provide insight on the *molecular-level* distribution of the two different linkers within the ZIF crystals. As recently shown, such understanding could be obtained in a specific MOF system through a combination of NMR spectroscopy and structure modeling.[32] The present work, on the other hand, is focused on demonstrating the role of linker substitution in obtaining large changes in adsorption and diffusion behavior.

Adsorption. Volumetric uptake profiles of *n*-butane and *i*-butane were collected at 308 K for five materials with x = 100, 63, 28, 7, and 0, representing decreasing ZIF-8 linker content and increasing effective pore size from pure ZIF-8 to pure ZIF-90. Figure S4a,b shows the adsorption isotherms obtained at equilibrated conditions up to a pressure of about 1.8 bar. The data are fitted to Langmuir isotherms. The fitted Langmuir capacity (C_s), affinity constant (b), and the Henry constant ($K = C_s \cdot b$) are tabulated in Table S1. There is a general increase in the Langmuir capacity and Henry constant with the fraction of ZIF-8 linkers, due to the more favorable interactions of alkanes with the methyl groups of the 2-MeIM linker. All the ZIF-8−90 materials slightly favor *i*-butane adsorption over *n*-butane. Overall, the adsorption properties show moderate changes as a function of x, as expected for adsorption of alkanes in ZIF materials which is governed by van der Waals interactions of the alkyl groups with the framework.

However, drastic changes are seen in the adsorption of water and alcohols upon tuning the ZIF-8−90 composition. Figure 3a shows water vapor adsorption isotherms in ZIF-8−90 materials at 308 K. It is clear that the hydrophobicity of ZIF materials can be tuned by controlling the composition of different linkers in the hybrid framework. As the fraction of hydrophilic carbonyl groups in the structure increases from pure ZIF-8 to pure ZIF-90, water

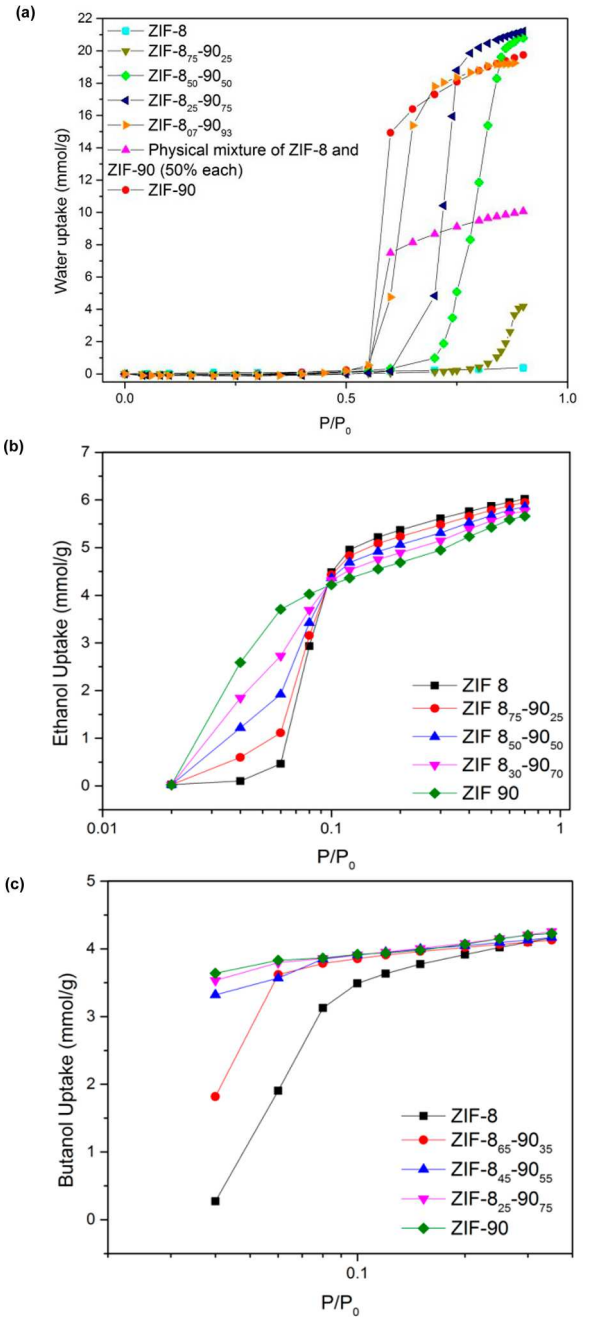

Figure 3. (a) Water adsorption isotherms in ZIF 8−90 hybrid crystals at 308 K, and the adsorption isotherm of a 50−50 (by mass) physical mixture of ZIF-8 and ZIF-90 crystals, (b) ethanol, and (c) *n*-butanol adsorption isotherms in ZIF 8−90 hybrid crystals at 308 K.

DOI: 10.1021/jacs.5b00803
J. Am. Chem. Soc. 2015, 137, 4191−4197

uptake starts to occur at lower relative pressures. The water adsorption isotherm for a physical 50−50 wt % mixture of ZIF-8 and ZIF-90 crystals is entirely different from that of a ZIF-8_{50}-90_{50} hybrid material. This is further corroboration that the 2-MeIm and OHC-Im linkers are forming true hybrid ZIFs. Figure 3b,c shows ethanol and *n*-butanol adsorption isotherms at 308 K. It is clear that the organophilicity of ZIFs can be tuned significantly, especially in the initial plateau region at low relative pressures, by adjusting the linker fraction (x). This region of low activity is significant for the concentration of alcohols (and other organics) from dilute aqueous solutions, a problem often encountered in biofuel and biobased chemical production.[33−35] For example, ethanol uptake into pure ZIF-8 only occurs at $P/P_0 > 0.06$. By progressively replacing methyl groups with carbonyl groups, the hybrid ZIF-8−90 framework attracts a much larger number of ethanol molecules at low pressures.

The isosteric heats (ΔH_{iso}) of ethanol adsorption for three materials, ZIF-8, ZIF-90, and ZIF 8_{50}−90_{50}, are shown in Figure S6. The data of $\ln(P)$ vs $1/T$ at constant loading was fitted at three different temperatures to obtain ΔH_{iso}. For ethanol (boiling point 351 K), the vapor sorption apparatus is only capable of measuring reliable isotherms at below 328 K (55 °C). Figure S7 illustrates the linearity between $\ln(P)$ and $1/T$ for ethanol adsorption in ZIF-8 for nine loadings at 298, 308, and 318 K. Similar results are also obtained for ZIF-90 and ZIF-8_{50}−90_{50}, and it is confirmed that the data points fit extremely well for ΔH_{iso} calculation with $R^2 > 0.98$ in all cases. From Figure S6, we find that ZIF-90 has the highest ΔH_{iso} at infinite dilution due to the polar −CHO group. Moreover, the ΔH_{iso} values increase slightly during ethanol uptakes up to 5 mmol/g for all three ZIFs. This indicates energetic homogeneity of the hybrid ZIF framework to ethanol adsorption and relatively weak adsorbate−adsorbate interactions in the low-pressure region. For ethanol uptake higher than 5 mmol/g, ΔH_{iso} increases more significantly with loading due to the more closely packed and hydrogen-bonded adsorbate molecules confined in the framework. The experimentally derived ΔH_{iso} values for pure ZIF-8 and ZIF-90 are in good agreement with existing molecular simulation data.[36]

The characteristic S-shape isotherms (Figure 3a,b) are not uncommon for ZIF materials with inherent structural flexibility that can undergo structural transformation induced by temperature, pressure, or guest molecules. The "gate-opening" effect, i.e., the reorientation of the imidazole linkers, was proposed to explain the inflections in experimental N_2 physisorption isotherms at 77 K.[37] The inflection points are at relative pressures of about 5×10^{-3} for ZIF-8 and about 10^{-4} for ZIF-90. However, the alcohol adsorption mechanism is different from that of cryogenic N_2 adsorption and is not related to the gate-opening effect. In ZIF-8, the gate-opening effect can only be obtained at high hydrostatic pressures or ultralow-pressure N_2 adsorption at 77 K.[22] More importantly, gate-opening is characterized by a hysteresis loop that marks the transformation between a less porous and a more porous phase induced by guest molecules.[38] Figure S8 shows representative adsorption and desorption branches at 323 K for water and ethanol in ZIF-8, ZIF-90, and ZIF-8_{50}−9_{50}. There is no desorption hysteresis, which indicates the S-shape isotherms are not due to the gate-opening effect but rather a cluster formation and cage-filling mechanism. In the case of ethanol sorption in ZIF-8, no desorption hysteresis was observed in a previous study.[26] The S-shape ethanol sorption isotherm in ZIF-71, a hydrophobic ZIF with RHO topology, has also been identified as a cluster formation and cage-filling mechanism via molecular simulations.[39] A more recent simulation study revealed that the cluster formation and cage-filling mechanism also holds for the adsorption of normal alcohols (methanol, ethanol, propanol, and butanol) in SOD-type ZIF materials such as ZIF-8.[36] At low loadings, the alcohol molecules form clusters at preferential adsorption sites around the organic linkers. With increasing vapor pressure, cage-filling occurs with a large saturation uptake of alcohol molecules. Framework flexibility has a negligible effect on equilibrium alcohol adsorption in ZIF-8 and ZIF-90.[24] These studies further corroborate our finding that the tunability of water and alcohol adsorption in hybrid ZIF-8−90 frameworks is a direct result of the tunable linker fractions and not an indirect result of changes in framework flexibility or gate-opening.

Diffusion. To clearly isolate the effect of pore tunability on molecular sieving in ZIF-8−90 materials, we again focus on the low-pressure regime wherein adsorbate−adsorbate interactions have minimal impact. In the case of the two hydrocarbon isomers *n*-butane and *i*-butane, the transport (i.e., Fickian) diffusivities are obtained by fitting the initial linear gravimetric uptake curves with an analytical model for uptake in spherical particles of given CSD (see Supporting Information for details of the methodology). To further elucidate the role of tunable molecular sieving, we obtain the corrected (Maxwell−Stefan, M-S) diffusivity from the transport diffusivity.[40] The M-S diffusivity captures the intrinsic rate of hopping of individual molecules through the pore windows of the material. Figure 4 shows the butane isomer transport diffusivities, M-S diffusivities, and the corresponding *n*-butane/*i*-butane diffusion selectivities of ZIF-8−90 materials. The data are also listed in Tables S2−S3. It is clear that the *n*-butane and *i*-butane transport diffusivities can be tuned continuously over 2−3 orders of magnitude by variation of the ZIF-8 linker fraction (x). The *n*-butane diffusion selectivity over

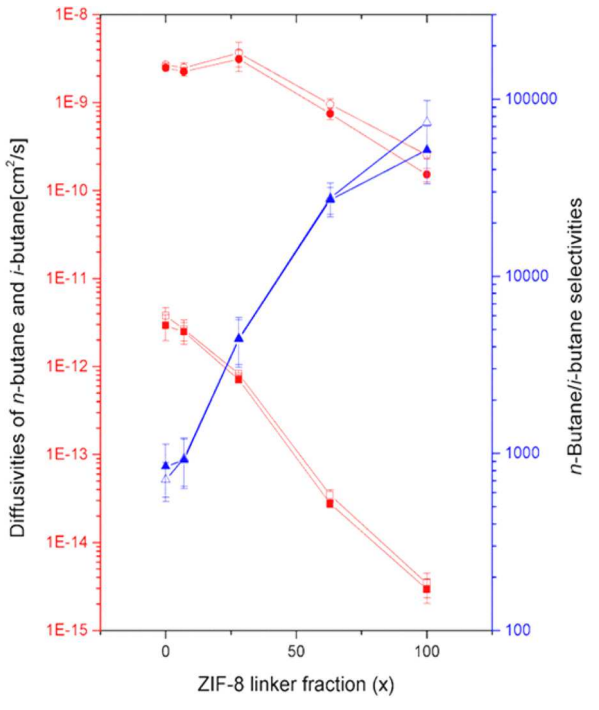

Figure 4. Fickian (open symbols) and corrected M-S (closed symbols) diffusivities of *n*-butane and *i*-butane (left axis), and the corresponding *n*-butane/*i*-butane selectivities (right axis) of ZIF 8−90 materials with varying values of x, measured at 308 K.

DOI: 10.1021/jacs.5b00803
J. Am. Chem. Soc. 2015, 137, 4191−4197

i-butane can be tuned between 900 and 50,000. A decreasing value of x leads to an increase in the effective pore size and allows faster hopping of both butane isomers through the pore windows. All the ZIF 8−90 materials have quite a sharp intrinsic selectivity for *n*-butane (kinetic diameter 0.43 nm) over *i*-butane (0.5 nm). However, several important considerations drive the selection of an optimum material for membrane-based separation of butane isomers based upon Figure 4. Materials close to ZIF-8 have impractically low *n*-butane diffusivities. Hence, materials closer to ZIF-90 are desired. The *n*-butane diffusivity appears to reach a plateau when x decreases below 28, whereas such an effect is not observed with *i*-butane. This is likely due to an uncertainty in determining accurate *n*-butane diffusivities in the larger-pore materials, due to fast *n*-butane diffusion and potential contamination of the data by external and surface mass transfer resistances even in the largest crystals used in this work. On the other hand, the data may also include a real effect, i.e., additional increase in the pore size at smaller values of x can no longer affect significantly the diffusion of the smaller hydrocarbon *n*-butane, whereas the larger *i*-butane continues to feel the limiting effect of the pore size. In either case, Figure 4 shows that materials close to ZIF-90 ($0 < x < 30$) are appropriate choices for *n*-butane/*i*-butane separation based on molecular sieving, since they combine high *n*-butane diffusivity ($>2 \times 10^{-9}$ cm^2/s) and high selectivity (at least 900−6000, considering the measured *n*-butane diffusivities as lower-bound values).

In the case of water and alcohols (Figure 5), the self-diffusivities of the three smaller molecules (water, methanol, and ethanol) were measured by PFG-NMR.[41] Due to their high diffusivities, gravimetric uptake measurements of diffusion were not feasible in these cases even with the largest crystals available. The PFG-NMR signal attenuation data were fitted to a double-exponential curve to obtain the self-diffusivity coefficient. The dominant fast diffusion component in the decay curve reflects the diffusion of the water/alcohol while the minor component has been attributed to a background signal from remaining solvent.[42,43] Representative fits are shown in Figure S9. The diffusivity of water in ZIF-8 was not measured due to its high hydrophobicity. The two bulkiest molecules (butanol and isobutanol) exhibited very poor signal-to-noise ratios in PFG-NMR data. This is due to the restricted rotational motion of the molecules, which manifests itself in a short transverse relaxation constant T_2. Hence, their M-S diffusivities were measured gravimetrically and the uptake data was analyzed using methods similar to those used for the hydrocarbon isomers (Supporting Information).

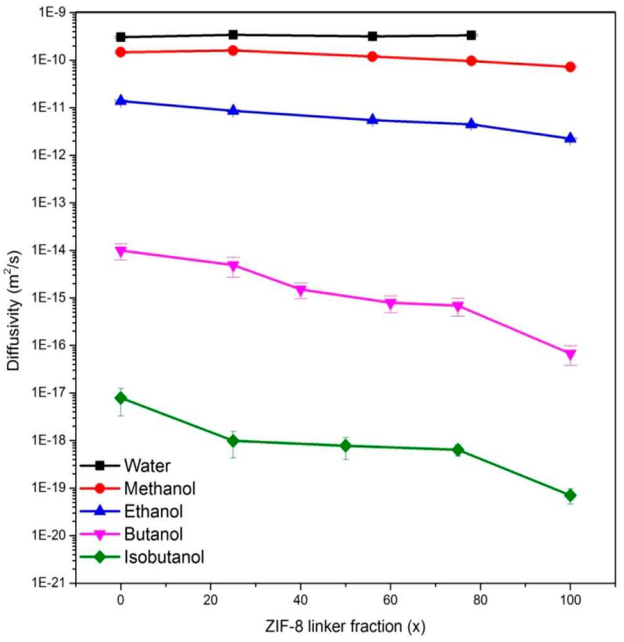

Figure 5. Self-diffusivities and M-S diffusivities of molecules in ZIF 8−90 hybrid materials. Water, methanol, and ethanol self-diffusivities are measured by PFG-NMR at 313 K. Butanol and isobutanol M-S diffusivities are measured by gravimetric uptake at 308 K.

Figure 5 shows that there is no appreciable change in water self-diffusivity for water as the linker composition is varied. This is due to the much smaller kinetic diameter of water (2.6 Å) in relation to the effective pore sizes of all the ZIF-8−90 materials. The diffusivity of methanol shows a small but systematic increase with decreasing ZIF-8 linker fraction. Ethanol shows an order-of-magnitude tunability of self-diffusivity and M-S diffusivity, whereas butanol and isobutanol show over two orders-of-magnitude tunability of the M-S diffusivity as a function of the linker composition. As the size of the diffusing molecule increases, the effective pore size has a more pronounced effect on the diffusivity at a given linker composition, as well as the sensitivity of the diffusivity to changes in the linker composition. This behavior strongly corroborates the molecular sieving nature of the observed diffusion characteristics in the mixed-linker ZIF-8−90 series. The self-diffusivities of methanol and ethanol in pure ZIF-8 and ZIF-90 are in good agreement with those measured previously by PFG-NMR.[24] The ethanol diffusivity in ZIF-8, previously measured using infrared microscopy,[42] also compares well with Figure 5. The diffusivity trend for isobutanol shows another interesting feature, which is the relatively smaller diffusivity change occurring in the x = 20−80 range. This is explained based on upon the fact that the effective pore sizes of the hybrid materials do not vary linearly as a function of composition. In previous work,[17] we measured the effective pore sizes of ZIF-8−90 materials by N_2 physisorption at 77 K and showed that it increased from 4.0 to 4.3 Å as x decreased from 100 to 76. Between x = 76 and 25, the increase in pore size is slower (from 4.3 to 4.5 Å). Thereafter, a large increase from 4.5 to 5.0 Å occurs over a small composition range between x = 25 and 0. With a kinetic diameter of 5.4 Å, isobutanol is by far the largest molecule among the set considered here. Due to its large size, its diffusion behavior follows the above trends in the effective pore size most closely. In other words, we observe the most significant changes in isobutanol diffusivity in the ZIF-8-rich and ZIF-90-rich regions ($x > 80$ or $x < 20$) and only moderate changes in the middle region.

CONCLUSION

We have demonstrated the continuous tuning of molecular sieving and adsorption behavior in mixed-linker ZIF-8−90 frameworks, which is due to the tunability of effective pore size as well as the ratio of polar and nonpolar functional groups in the framework. These results are facilitated by the synthesis of a range of ZIF-8−90 mixed linker materials with average crystal sizes spanning from 338 nm to almost 100 μm and the detailed determination of the CSDs. Micro-Raman composition analysis of individual ZIF-8−90 crystals conclusively shows the hybrid nature and high uniformity of the mixed-linker materials. Tunable molecular sieving is observed both in nonpolar alkanes as well in strongly polar alcohols, whereas tunable adsorption behavior is primarily observed for polar molecules like water and

DOI: 10.1021/jacs.5b00803
J. Am. Chem. Soc. 2015, 137, 4191−4197

alcohols. The *n*-butane and *i*-butane diffusivities and the *n*-butane/*i*-butane diffusion selectivity can be continuously tuned over several orders of magnitude, allowing the selection of suitable materials for membrane-based separation of these isomers. Diffusion measurements of water and alcohols also reveal the strong dependence of diffusivity on the molecular sizes and tunable ZIF-8−90 pore sizes. The adsorption affinities of water and alcohols at low pressures are also strongly tunable by the variation of linker composition. This detailed demonstration of tunable adsorption and diffusion properties in ZIF-8−90 materials opens up the wider applicability of mixed-linker ZIF materials as a platform for a variety of membrane- and adsorption-based molecular separations.

■ ASSOCIATED CONTENT

Supporting Information

Details of mixed-linker ZIF synthesis, particle size distributions, XRD patterns, FT-Raman peak assignments, hydrocarbon adsorption isotherms, Langmuir fit parameters, ethanol and water adsorption isotherms, ethanol isosteric heats of adsorption, methodology for obtaining transport diffusivities, Maxwell−Stefan diffusivities from volumetric or gravimetric uptake data, tables of hydrocarbon diffusivities, methodology for obtaining diffusivities from PFG-NMR data, and methodology for obtaining isosteric heat of adsorption from adsorption isotherms. This material is available free of charge via the Internet at http://pubs.acs.org.

■ AUTHOR INFORMATION

Corresponding Author

*sankar.nair@chbe.gatech.edu

Author Contributions

‖These authors contributed equally.

Notes

The authors declare no competing financial interest.

■ ACKNOWLEDGMENTS

This work was supported by Phillips 66 Company, the National Science Foundation (CBET-1264874 and CBET-0966582), the Department of Energy (DE-FOA-0000096), and Algenol Biofuels.

■ REFERENCES

(1) Shah, M.; McCarthy, M. C.; Sachdeva, S.; Lee, A. K.; Jeong, H.-K. *Ind. Eng. Chem. Res.* **2011**, *51*, 2179−2199.

(2) Bux, H.; Feldhoff, A.; Cravillon, J.; Wiebcke, M.; Li, Y.-S.; Caro, J. *Chem. Mater.* **2011**, *23*, 2262−2269.

(3) Farha, O. K.; Özgür Yazaydın, A.; Eryazici, I.; Malliakas, C. D.; Hauser, B. G.; Kanatzidis, M. G.; Nguyen, S. T.; Snurr, R. Q.; Hupp, J. T. *Nat. Chem.* **2010**, *2*, 944−948.

(4) Demessence, A.; D'Alessandro, D. M.; Foo, M. L.; Long, J. R. *J. Am. Chem. Soc.* **2009**, *131*, 8784−8786.

(5) Cohen, S. M. *Chem. Rev.* **2011**, *112*, 970−1000.

(6) Pan, L.; Olson, D. H.; Ciemnolonski, L. R.; Heddy, R.; Li, J. *Angew. Chem.* **2006**, *118*, 632−635.

(7) Getman, R. B.; Bae, Y.-S.; Wilmer, C. E.; Snurr, R. Q. *Chem. Rev.* **2011**, *112*, 703−723.

(8) Zhang, C.; Dai, Y.; Johnson, J. R.; Karvan, O.; Koros, W. J. *J. Membr. Sci.* **2012**, *389*, 34−42.

(9) Kwon, H. T.; Jeong, H.-K. *J. Am. Chem. Soc.* **2013**, *135*, 10763−10768.

(10) Liu, D.; Ma, X.; Xi, H.; Lin, Y. S. *J. Membr. Sci.* **2014**, *401*−*402*, 76−82.

(11) Pan, Y.; Lai, Z. *Chem. Commun.* **2011**, *47*, 10275−10277.

(12) Phan, A.; Doonan, C. J.; Uribe-Romo, F. J.; Knobler, C. B.; O'Keeffe, M.; Yaghi, O. M. *Acc. Chem. Res.* **2009**, *43*, 58−67.

(13) Banerjee, R.; Phan, A.; Wang, B.; Knobler, C. B.; Furukawa, H.; O'Keeffe, M.; Yaghi, O. M. *Science* **2008**, *319*, 939−943.

(14) Park, K. S.; Ni, Z.; Cote, A. P.; Choi, J. Y.; Huang, R.; Uribe-Romo, F. J.; Chae, H. K.; O'Keeffe, M.; Yaghi, O. M. *Proc. Natl. Acad. Sci. U.S.A.* **2006**, *103*, 10186−10191.

(15) Li, J.-R.; Kuppler, R. J.; Zhou, H.-C. *Chem. Soc. Rev.* **2009**, *38*, 1477−1504.

(16) Li, J.-R.; Ma, Y.; McCarthy, M. C.; Sculley, J.; Yu, J.; Jeong, H.-K.; Balbuena, P. B.; Zhou, H.-C. *Coord. Chem. Rev.* **2011**, *255*, 1791−1823.

(17) Thompson, J. A.; Blad, C. R.; Brunelli, N. A.; Lydon, M. E.; Lively, R. P.; Jones, C. W.; Nair, S. *Chem. Mater.* **2012**, *24*, 1930−1936.

(18) Brown, A. J.; Brunelli, N. A.; Eum, K.; Rashidi, F.; Johnson, J. R.; Koros, W. J.; Jones, C. W.; Nair, S. *Science* **2014**, *345*, 72.

(19) Qiu, S.; Xue, M.; Zhu, G. *Chem. Soc. Rev.* **2014**, *43*, 6116−6140.

(20) Pan, Y.; Li, T.; Lestari, G.; Lai, Z. *J. Membr. Sci.* **2012**, *390*−*391*, 93−98.

(21) Krishna, R. *Chem. Soc. Rev.* **2012**, *41*, 3099−3118.

(22) Zhang, K.; Lively, R. P.; Zhang, C.; Chance, R. R.; Koros, W. J.; Sholl, D. S.; Nair, S. *J. Phys. Chem. Lett.* **2013**, *4*, 3618−3622.

(23) Zhang, C.; Lively, R. P.; Zhang, K.; Johnson, J. R.; Karvan, O.; Koros, W. J. *J. Phys. Chem. Lett.* **2012**, *3*, 2130−2134.

(24) Gee, J. A.; Chung, J.; Nair, S.; Sholl, D. S. *J. Phys. Chem. C* **2013**, *117*, 3169−3176.

(25) Zhang, K.; Lively, R. P.; Dose, M. E.; Brown, A. J.; Zhang, C.; Chung, J.; Nair, S.; Koros, W. J.; Chance, R. R. *Chem. Commun.* **2013**, *49*, 3245.

(26) Zhang, K.; Lively, R. P.; Zhang, C.; Koros, W. J.; Chance, R. R. *J. Phys. Chem. C* **2013**, *117*, 7214−7225.

(27) Thompson, J. A.; Brunelli, N. A.; Lively, R. P.; Johnson, J. R.; Jones, C. W.; Nair, S. *J. Phys. Chem. C* **2013**, *117*, 8198−8207.

(28) Zimmerman, C. M.; Singh, A.; Koros, W. J. *J. Polym. Sci. B: Polym. Phys.* **1998**, *36*, 1747−1755.

(29) Karger, J.; Ruthven, D. M.; Theodorou, D. N. In *Diffusion in Nanoporous Materials*, 1st ed., . Wiley-VCH Verlag & Co. KGaA: Weinheim, Germany, 2012; Vol. *1*, pp 426−436.

(30) Cravillon, J.; Münzer, S.; Lohmeier, S.-J.; Feldhoff, A.; Huber, K.; Wiebcke, M. *Chem. Mater.* **2009**, *21*, 1410−1412.

(31) Cravillon, J.; Schroder, C. A.; Bux, H.; Rothkirch, A.; Caro, J.; Wiebcke, M. *CrystEngComm* **2012**, *14*, 492−498.

(32) Kong, X.; Deng, H.; Yan, F.; Kim, J.; Swisher, J. A.; Smith, B.; Yaghi, O. M.; Reimer, J. A. *Science* **2013**, *341*, 882−885.

(33) Hill, A. E.; Malisoff, W. M. *J. Am. Chem. Soc.* **1926**, *48*, 918−927.

(34) Kumar, M.; Gayen, K. *Appl. Energy* **2011**, *88*, 1999−2012.

(35) Qin, F.; Li, S.; Qin, P.; Karim, M. N.; Tan, T. *Green Chem.* **2014**, *16*, 1262−1273.

(36) Zhang, K.; Zhang, L.; Jiang, J. *J. Phys. Chem. C* **2013**, *117*, 25628−25635.

(37) Fairen-Jimenez, D.; Moggach, S. A.; Wharmby, M. T.; Wright, P. A.; Parsons, S.; Duren, T. *J. Am. Chem. Soc.* **2011**, *133*, 8900−8902.

(38) Pera-Titus, M.; Farrusseng, D. *J. Phys. Chem. C* **2012**, *116*, 1638−1649.

(39) Nalaparaju, A.; Zhao, X. S.; Jiang, J. W. *J. Phys. Chem. C* **2010**, *114*, 11542−11550.

(40) Krishna, R.; Baur, R. *Sep. Purif. Technol.* **2003**, *33*, 213−254.

(41) Callaghan, P. T. *Translational dynamics and magnetic resonance: Principles of pulsed gradient spin echo NMR*; Oxford University Press: Oxford, U.K., 2011.

(42) Karger, J.; Ruthven, D. M.; Theodorou, D. In *Diffusion in Nanoporous Materials*; Wiley-VCH Verlag & Co. KGaA: Weinheim, Germany, 2012; Vol. *2*, pp 739−744.

(43) Stallmach, F.; Gröger, S.; Künzel, V.; Kärger, J.; Yaghi, O. M.; Hesse, M.; Müller, U. *Angew. Chem., Int. Ed.* **2006**, *45*, 2123−2126.

DOI: 10.1021/jacs.5b00803
J. Am. Chem. Soc. 2015, 137, 4191−4197